

Dynamic Test-Time Compute Scaling in Control Policy: Difficulty-Aware Stochastic Interpolant Policy

Inkook Chun[†] Seungjae Lee[‡] Michael S. Albergo[◊]

Saining Xie[†] Eric Vandenberg-Eijnden^{†,§}

[†]New York University [‡]University of Maryland

[◊]Harvard University [§]Capital Fund Management

Abstract

Diffusion- and flow-based policies deliver state-of-the-art performance on long-horizon robotic manipulation and imitation learning tasks. However, these controllers employ a **fixed inference budget at every control step**, regardless of task complexity, leading to computational inefficiency for simple subtasks while potentially underperforming on challenging ones. To address these issues, we introduce *Difficulty-Aware Stochastic Interpolant Policy (DA-SIP)*, a framework that enables robotic controllers to **adaptively adjust their integration horizon in real time** based on task difficulty. Our approach employs a *difficulty classifier* that analyzes observations to dynamically select the step budget, the optimal solver variant, and ODE/SDE integration at each control cycle. DA-SIP builds upon the stochastic interpolant formulation to provide a unified framework that unlocks diverse training and inference configurations for diffusion- and flow-based policies. Through comprehensive benchmarks across diverse manipulation tasks, DA-SIP achieves **2.6–4.4× reduction in total computation time** while maintaining task success rates comparable to fixed maximum-computation baselines. By implementing adaptive computation within this framework, DA-SIP transforms generative robot controllers into efficient, task-aware systems that intelligently allocate inference resources where they provide the greatest benefit.

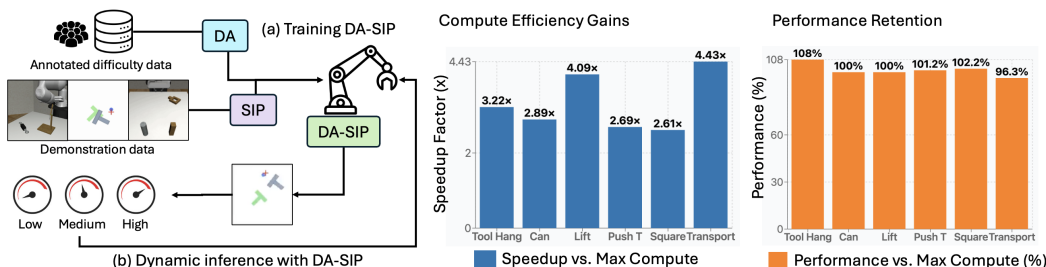


Figure 1: Overview of the DA-SIP framework with computational efficiency gains and performance retention

1 Introduction

Diffusion [1, 2] and flow-matching [3–5] models have recently shown strong performance in imitation learning for robotic policies, producing long-horizon action plans. By iteratively denoising trajectories (diffusion) or integrating probability-flow ODEs (flows), they capture the multi-modal distributions present in human demonstrations. These policies can be coupled with Vision-Language Models

(VLMs) to form *Vision-Language-Action models* (VLAs) that map natural language goals to low-level control [6, 7].

Despite their success, existing controllers adopt a **uniform inference budget**: every control cycle executes the same solver, step schedule, and interpolant—all chosen to handle the **hardest** subtasks. This wastes computation on easy subtasks while ignoring a key advantage of flow-based generative models: the solver type, step count, and ODE/SDE formulation can all be adjusted at test time without retraining.

Large language models already employ adaptive computation: they use more reasoning steps for difficult queries and fewer for simple ones [8]. Physical manipulation tasks exhibit similar heterogeneity: coarse motions (e.g., moving an arm in free space) can be planned with minimal computation, while sub-millimeter placements demand more computational resources for precision.

To address this gap, we develop *Difficulty-Aware Stochastic Interpolant Policy* (DA-SIP), which uses difficulty classification to dynamically allocate computational resources within the stochastic interpolant framework. Unobstructed object approaches receive minimal computational budgets, while precision manipulations command substantially higher budgets to ensure optimal performance.

This adaptive mechanism incorporates a dataset of demonstrations annotated with subtask difficulty levels. These annotations are used to train three complementary difficulty classifiers: (i) a lightweight CNN designed for efficiency, (ii) a few-shot vision-language model (VLM) prompted with exemplar images, and (iii) a few-shot VLM fine-tuned on our collected data. During each control cycle, the selected classifier evaluates the current observation and predicts a difficulty level.

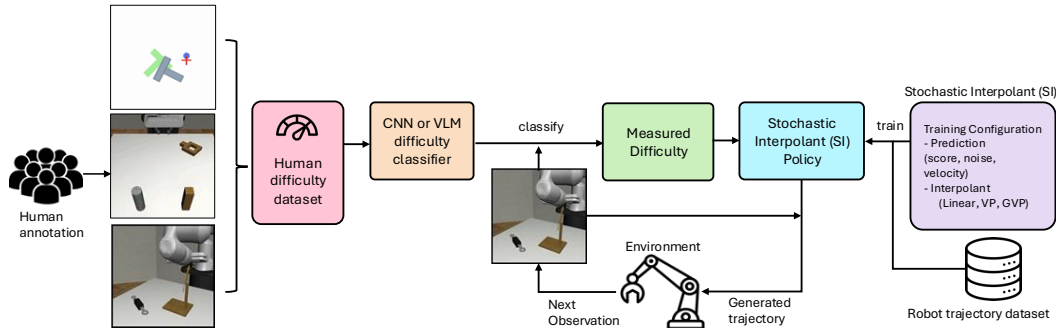


Figure 2: High-level overview of our difficulty-aware stochastic interpolant policy (DA-SIP) framework. During training we choose (1) a prediction target (noise, score, or velocity), (2) an interpolant (Linear, VP, GVP, *etc.*), and this configuration yields a single generative policy network that can perform both ODE and SDE integration. At inference time, a learned difficulty classifier adaptively selects an inference configuration triple \langle step count, solver type, ODE/SDE formulation \rangle based on the current state—enabling context-dependent “System 1 vs. System 2” compute that maximizes success while minimizing latency.

To implement this adaptive computation effectively, we ground our approach in the *stochastic interpolant* (SI) framework [9], which unifies flow-based (ODE) and diffusion-based (SDE) generative modeling. This formulation enables a critical capability: translating difficulty levels into optimized inference configurations. Specifically, each difficulty level determines an inference configuration \langle step count, solver type, ODE/SDE integration \rangle , allowing the system to dynamically adjust computational resources (Fig. 2).

Contributions.

1. **SI-grounded generative policy framework.** We unify diffusion and flow policies under stochastic interpolants, *exposing* a spectrum of training and inference choices in continuous time.
2. **Difficulty-aware adaptive compute.** The difficulty classifier selects solver type and step count using a lightweight CNN, few-shot VLM, or fine-tuned VLM, yielding a **2.6–4.4 \times** compute reduction without sacrificing success rate.

3. **Comprehensive benchmark study.** We demonstrate that our difficulty-guided approach reduces task completion time while matching the success rate of the maximum-compute baseline, and we analyze the resulting latency-accuracy trade-off.

2 Related Work

Generative models Modern generative modeling techniques include diffusion models [1, 2, 10], flow matching [3–5], and stochastic interpolants that unify both frameworks [9, 11]. Diffusion models iteratively denoise data using score-matching objectives, while flow matching directly trains neural ODEs along flexible interpolation paths [3]. Recent distillation techniques further enhance computational efficiency [12–15]. The *stochastic interpolant* framework **uncouples the interpolation trajectory from the choice of deterministic (ODE) or stochastic (SDE) dynamics**, clarifying the design space and enabling independent control over sample quality, speed, and robustness.

Generative modeling for decision making Diffusion Policy adapts diffusion-based generative modeling to learn robot control policies from human demonstrations [16]. Generating action sequences rather than single actions has demonstrated strong performance [17]. Flow-matching policies model the flow from noise to expert behavior through continuous transformations [18]. Moreover, distillation methods for control policies have been introduced [19, 20]. AdaFlow measures the multimodality of the action space in imitation learning by estimating the variance of possible actions at each state [21]. While it introduces adaptation by measuring multimodality in the action space, it addresses only a single dimension of state complexity-variance. In contrast, our approach recognizes multiple dimensions of state difficulty and provides a more comprehensive adaptation framework built on the stochastic interpolant framework, adjusting the full inference triplet: step count, solver type, and ODE/SDE integration mode.

LLMs and VLMs for Robotic Control Recent work has integrated large language and vision-language models into robot control, creating Vision-Language-Action (VLA) models that map natural language and visual observations to control actions [7, 22, 23]. SayCan [24] grounds LLMs by constraining language outputs to feasible robot skills, while Inner Monologue [25] enables closed-loop reasoning where environmental feedback guides task execution. Our difficulty-aware approach in DA-SIP implements adaptive computation at the action generation level, conceptually similar to how LLMs allocate more “thinking” steps to complex queries [8], but applied to the visual control domain.

3 Methods

3.1 Generating Flow Policies with Stochastic Interpolants

Flow- and diffusion-based policies transform standard Gaussian noise $\varepsilon \sim \mathcal{N}(\mathbf{0}, \mathbf{I})$ into a sequence of robot actions $\mathbf{x}_* \sim p(\mathbf{x} \mid \mathbf{o})$, where \mathbf{o} are observations. Here we do so within the stochastic interpolant framework [9]. To this end, we first introduce the **stochastic interpolant**

$$\mathbf{I}_t = \alpha_t \mathbf{x}_* + \sigma_t \varepsilon, \quad t \in [0, 1], \quad (1)$$

where α_t decreases from $\alpha_0 = 1$ to $\alpha_1 = 0$ and σ_t increases from $\sigma_0 = 0$ to $\sigma_1 = 1$, thereby interpolating between the action sequence $\mathbf{I}_0 = \mathbf{x}_*$ at $t = 0$ and pure noise $\mathbf{I}_1 = \varepsilon$ at $t = 1$.

Associated with the stochastic interpolant (1) we define the **velocity field**

$$\mathbf{v}(\mathbf{x}, t, \mathbf{o}) = \mathbb{E}[\dot{\mathbf{I}}_t \mid \mathbf{I}_t = \mathbf{x}, \mathbf{o}] \quad (2)$$

where $\mathbb{E}[\cdot \mid \mathbf{I}_t = \mathbf{x}, \mathbf{o}]$ denotes the expectation over \mathbf{x}_* , ε conditional on $\mathbf{I}_t = \mathbf{x}$ and \mathbf{o} fixed. This velocity can be efficiently learned by minimizing the loss

$$L_v[\hat{\mathbf{v}}] = \mathbb{E}[|\hat{\mathbf{v}}(\mathbf{I}_t, t, \mathbf{o}) - \dot{\mathbf{I}}_t|^2], \quad (3)$$

where the expectation is taken over \mathbf{x}_* , ε , \mathbf{o} and $t \sim U(0, 1)$.

The **score** of the probability density of the interpolant (i.e. the gradient of the logarithm of this density) is given, via Stein’s relation, as

$$s(\mathbf{x}, t, \mathbf{o}) = -\sigma_t^{-1} \mathbb{E}[\varepsilon \mid \mathbf{I}_t = \mathbf{x}, \mathbf{o}] \quad (4)$$

which can be learned by minimizing the loss

$$L_s[\hat{\mathbf{s}}] = \mathbb{E}[|\hat{\mathbf{s}}(\mathbf{I}_t, t, \mathbf{o}) + \sigma_t^{-1}\boldsymbol{\varepsilon}|^2], \quad (5)$$

Alternatively, the score can be expressed in terms of the velocity (2) and *vice-versa* as

$$\mathbf{s}(\mathbf{x}, t, \mathbf{o}) = \sigma_t^{-1} \frac{\alpha_t \mathbf{v}(\mathbf{x}, t, \mathbf{o}) - \dot{\alpha}_t \mathbf{x}}{\dot{\alpha}_t \sigma_t - \alpha_t \dot{\sigma}_t} \Leftrightarrow \mathbf{v}(\mathbf{x}, t, \mathbf{o}) = \frac{\alpha_t}{\dot{\alpha}_t} \mathbf{x} + \frac{\sigma_t(\dot{\alpha}_t \sigma_t - \alpha_t \dot{\sigma}_t)}{\alpha_t} \mathbf{s}(\mathbf{x}, t, \mathbf{o}) \quad (6)$$

These equations can be obtained by combining (2) and (4) with the relation $\mathbf{x} = \mathbb{E}[\mathbf{I}_t \mid \mathbf{I}_t = \mathbf{x}, \mathbf{o}]$, decomposing the conditional expectation of the sums into a sum of conditional expectations, and solving for $\mathbf{s}(\mathbf{x}, t, \mathbf{o})$ or $\mathbf{v}(\mathbf{x}, t, \mathbf{o})$.

Finally, we introduce the **reverse-time SDE**:

$$d\mathbf{X}_t = \left[\mathbf{v}(\mathbf{X}_t, t, \mathbf{o}) - \frac{1}{2} w_t s(\mathbf{X}_t, t, \mathbf{o}) \right] dt + \sqrt{w_t} d\bar{\mathbf{W}}_t, \quad \mathbf{X}_1 = \boldsymbol{\varepsilon} \quad (7)$$

where $w_t \geq 0$ is a diffusion coefficient that can be adjusted post-training and $\bar{\mathbf{W}}_t$ is a reverse Wiener process. The probability distribution of the solution to (7) conditional on \mathbf{o} coincides at all times with the probability distribution of the interpolant conditional on \mathbf{o} . In particular, the distribution of \mathbf{X}_0 is the target distribution $p(\mathbf{x} \mid \mathbf{o})$, indicating that (7) can be used as a generative model of sequence of robot actions given observations. The unconditional case is recovered by dropping the conditioning on \mathbf{o} .

In practice, we instantiate the equations above using **three stochastic interpolants** with different choices of α_t and σ_t :

Linear	Variance-Preserving (VP)	generalized VP (GVP)
$\alpha_t = t$, $\sigma_t = 1 - t$.	$\alpha_t = \sqrt{1 - \exp\left(-\int_0^t \beta_s ds\right)}$, $\sigma_t = \exp\left(-\frac{1}{2} \int_0^t \beta_s ds\right)$.	$\alpha_t = \sin\left(\frac{\pi}{2}t\right)$, $\sigma_t = \cos\left(\frac{\pi}{2}t\right)$.

These stochastic interpolants correspond to different ways to interpolate between noise and action sequences. Linear interpolation provides a direct, computationally efficient path; VP interpolation, up to time rescaling, recovers the formulation used in diffusion models; and GVP’s trigonometric formulation ensures analytical normalization ($\alpha_t^2 + \sigma_t^2 = 1$).

3.2 Difficulty Classification Methods

We explore three approaches for classifying subtask difficulty from observations, ranging from lightweight neural networks to vision-language models.

1. **Lightweight CNN Classifier.** A ResNet-18 backbone with a classification head processes observations to predict difficulty levels. This supervised approach is trained on 300 annotated images per task (from a total dataset of ~ 2000 timesteps per task), providing efficient real-time classification with minimal computational overhead (~ 20 ms per inference).
2. **Few-Shot VLM Classifier.** This zero-training approach leverages pre-trained vision-language models prompted with 1–3 exemplar images per difficulty category. The VLM classifies the current observation by comparing it to the provided examples, requiring no task-specific training but incurring higher inference latency (~ 500 –1000ms).
3. **Fine-Tuned VLM Classifier.** We fine-tune a pre-trained vision-language model on our annotated difficulty dataset (300 training images per task). This approach combines the strong representational capacity of VLMs with improved inference speed (~ 300 –400ms) and achieves the highest classification accuracy across tasks.

3.3 Adaptive Computation Allocation

At each control step, the difficulty classifier outputs a difficulty level $d(\mathbf{o}_t) \in \{1, 2, 3\}$ for the current observation \mathbf{o}_t . This difficulty level is mapped to an *inference configuration triple*

$$(N_t, \text{solver}_t, \text{type}_t) = \mathcal{M}(d(\mathbf{o}_t)),$$

where $N_t \in \{5, 10, 20\}$ is the number of integration steps, $\text{solver}_t \in \{\text{Euler}, \text{Heun}, \text{RK4}\}$ specifies the numerical integrator, and $\text{type}_t \in \{\text{ODE}, \text{SDE}\}$ determines the integration mode. The mapping \mathcal{M} is determined empirically by evaluating performance-efficiency trade-offs on a validation set. The configuration triple is then used by the Stochastic Interpolant Policy (SIP) to generate the next action sequence:

$$\mathbf{x} \sim \text{SIP}(\mathbf{o}_t; N_t, \text{solver}_t, \text{type}_t).$$

Computational efficiency. For our three-level difficulty system, we map difficulty levels to configurations that balance performance and compute cost:

- **Easy** ($d = 1$): ($N = 5$, Euler, ODE) — minimal computation for coarse motions
- **Medium** ($d = 2$): ($N = 10$, Heun, ODE) — moderate resources for approach phases
- **Hard** ($d = 3$): ($N = 20$, RK4, SDE) — maximum computation for precision tasks

This adaptive allocation enables the system to use minimal resources for simple subtasks while reserving expensive high-fidelity integration for challenging manipulation phases.

4 Experiments and Results

We evaluate our adaptive flow policy framework across various robotic manipulation tasks to demonstrate its versatility and effectiveness.

4.1 Simulation Environments

Our evaluation spans diverse simulation environments:

- **RoboMimic**: Benchmark suite for imitation learning in manipulation (Can, Lift, Square, Tool Hang tasks) [26]
- **Block Push**: A non-prehensile manipulation task (from the Fetch suite) in which a 7-DoF arm must push a cubic block across a tabletop to a target pose, requiring precise contact planning and continuous control [27]
- **Push-T**: Precision manipulation task requiring continuous control [28]
- **Kitchen**: Multi-stage environment with sequential task completion [29]
- **Multimodal Ant**: Locomotion tasks requiring complex coordination [30]

These environments represent a spectrum of complexity, from simple locomotion to intricate multi-object manipulation.

4.2 Optimizing Solver Configurations for Diverse Robotic Tasks

For uniformity and fair comparison across baselines, we focus on *velocity* prediction, although our framework also supports *score* prediction as an alternative training target [2, 4]. Our experiments reveal that different robotic tasks require distinct solver configurations to achieve optimal performance, as summarized in Table 1. Our adaptive computation mechanism draws inspiration from adaptive inference in neural networks [8] and builds upon recent advances in flow-based policy learning [18, 20, 31–33].

Our systematic evaluation revealed a key finding: there is no single best configuration that universally outperforms others across all environments. Initially, we hypothesized that evaluating all possible training and inference configurations of the stochastic interpolant framework would yield one optimal configuration outperforming all others across tasks. Instead, we discovered that different tasks require fundamentally different configurations to achieve optimal performance.

Simple manipulation tasks. Simple tasks like Can and Lift achieve near-optimal performance with minimal computation, with even 1-step configurations reaching 99–100% success. Even single-step flow model inference without distillation achieves the highest maximum performance, indicating that additional inference computation is wasted.

Table 1: Task characterisation and optimal configurations.

Task	PushT	Block Push	Tool Hang	Multimodal Ant	Lift	Can	Transport	Square
Solver	Heun	Heun	Euler	Euler	Euler	Euler	Euler	Euler
Interpolation	VP	GVP	VP	VP	Linear	Linear	VP	VP
Integration	SDE	SDE	ODE	ODE	ODE	ODE	SDE	SDE
Inference steps	100	100	50	25	1	1	100	100
Last step	Tweedie	Tweedie	None	None	None	None	Euler	Euler
Success rate (%)	92.6	22.8	38.1	45.3	100.0	100.0	85.0	95.2

Each configuration is trained for 5,000 epochs with three random training seeds. The model uses a U-Net transformer architecture. During evaluation, we use three inference seeds per training seed (nine runs per configuration). Checkpoints are saved every 50 epochs, and we report the mean success rate of the final 10 checkpoints, with each checkpoint evaluated over 50 independent episodes. Training is performed on NVIDIA L40S GPUs.

Precision manipulation tasks. Push-T and Block Push demonstrate strong dependency on the integration method. These tasks require substantially more computational resources because millimeter-precision actions produce meaningful differences in success rates. Heun approximation outperforms Euler by a slight margin ($\pm 0.1\%$) consistently across different training and inference seeds, highlighting the importance of accurate numerical integration for high-precision control tasks.

Exploratory manipulation tasks. Most notably, Tool Hang and Multimodal Ant tasks achieve peak performance at intermediate step counts. Increasing from the optimal step count (50 for Tool Hang, 25 for Multimodal Ant) to 100 steps actually decreases performance by 0.5–2.9%, suggesting that excessive computation can be counterproductive. We attribute this phenomenon to the need for controlled stochasticity in exploratory manipulation—similar to threading a needle, where some variation aids success but excessive randomness becomes detrimental.

Transport and placement tasks. Square and Transport tasks represent a middle ground, requiring neither the minimal computation of simple tasks nor the extreme precision of complex ones. While they involve multiple sequential actions, they don’t demand the millimeter-level precision or carefully controlled stochasticity of the more challenging environments.

This diversity in optimal configurations reinforces our understanding that different robotic tasks have distinct computational requirements, motivating adaptive methods that adjust computational resources based on task characteristics.

4.3 Categorizing Tasks by Difficulty

In all tasks, we identify distinct phases through which the robot progresses. When the robot is initialized far from interaction objects, we categorize this as the **Initial** state (I). As the robot approaches within approximately 10 cm of an object, we designate this as the **Near** state (N). Subsequently, the robot engages in one of three interaction types: **Grasping** (G), where the robot grasps and places an object; **Stochastic attempts** (S), which require exploratory variability for precise placement; or **Continuous pushing** (C), where the robot pushes objects without grasping.

By categorizing tasks based on manipulation type to assign an appropriate difficulty level, we avoid the need to find optimal configurations for each individual task, which would be impractical. We use a standardized categorization system that can be applied uniformly across all tasks. This one-time categorization eliminates any additional per-task tuning at deployment.

4.4 Difficulty Classification Performance

We developed a methodology to reliably categorize states across our environments. We collected annotations from 8 different human labelers, accumulating approximately 20,000 labeled states across the six difficulty categories (I, N, G, S, C, E). Our ablation studies show that 300 images per task prove sufficient (Appendix E.1). For each state, we assigned the final label based on majority voting, selecting the category with the highest frequency of votes among annotators. This consensus-driven

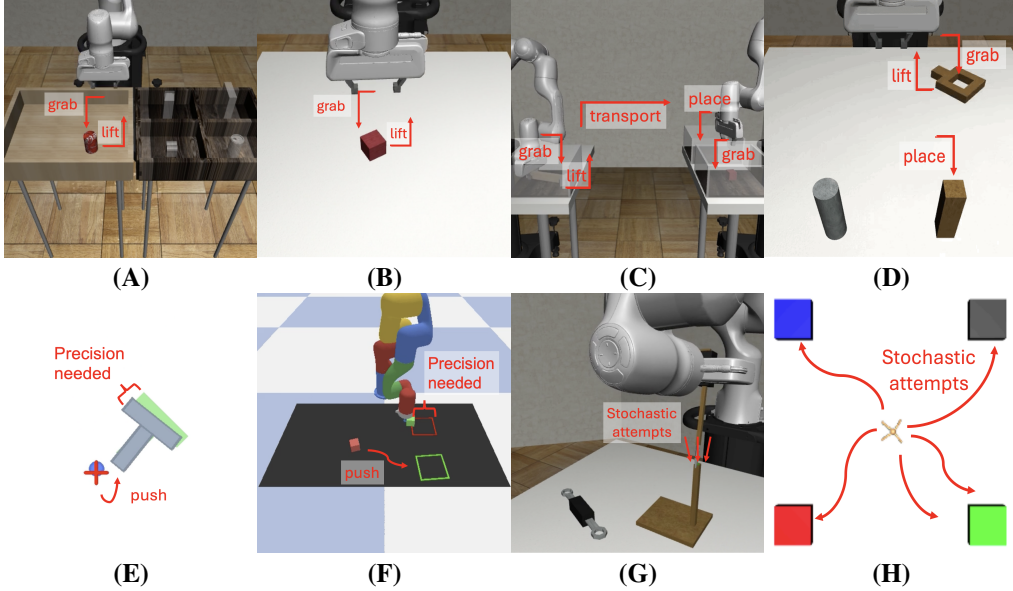


Figure 3: **Robot manipulation tasks across complexity categories.** (A-B) Simple manipulation tasks (*Can* and *Lift*) require minimal computational steps while maintaining high success rates. (C-D) Transport and placement tasks (*Transport* and *Square*) show greater sensitivity to configuration choices, representing medium-complexity challenges. (E-F) Precision manipulation tasks (*Push T* and *Block Push*) demonstrate significant benefits from Heun integration and variance-preserving diffusion models for fine-grained control. (G-H) Exploratory manipulation tasks (*Tool Hang* and *Multimodal Ant*) highlight that adaptive resource allocation outperforms maximum computation, addressing complex challenges with varying difficulty levels.

approach helped mitigate individual biases while establishing a comprehensive ground truth dataset. Additionally, we selected a small representative subset (1–3 images per category) for few-shot prompting with vision-language models (VLMs). We fine-tuned several VLMs on our dataset and selected the best-performing model for classification (Table 2).

(a) Lightweight CNN accuracy

Env.	Acc. (%)
Can	88.9
Lift	92.8
Push-T	94.6
Square	87.4
Tool Hang	81.3
Transport	91.5

(b) Few-shot VLM average

VLM	Avg. (%)
LLAVA	25.0
Gemma-3	23.0
Phi-4	24.6
Qwen2.5	45.3
Qwen2.5 (Fine-tuned)	53.9

(c) Qwen-VL 2.5 per-env.

Env.	Few-shot (%)	Fine-tuned (%)
Can	37.5	47.5
Lift	83.3	86.7
Push-T	42.0	56.7
Square	26.0	52.0
Tool Hang	50.0	40.0
Transport	30.0	40.0

Table 2: Difficulty classifier accuracy. We test different models [34–36]. For CNN, our ablation studies in Appendix E.1 show that approximately 300 images per task achieve near-plateau performance, requiring only about 15 minutes of annotation effort per task. The CNN classifier also demonstrates robustness to sensor noise (Appendix E.4). For the few-shot VLM, the impact of varying numbers of exemplar images is described in Appendix E.3.

Our lightweight CNN classifier demonstrated the strongest performance across all environments in both accuracy and inference time. Among the tested VLMs, Qwen-VL 2.5 achieved the highest average accuracy (45.3%) for few-shot multi-image prompting. We fine-tuned this VLM for 8 epochs, and fine-tuning with a minimal number of images further boosted accuracy (Table 2).

4.5 Assigning inference triplets based on difficulty label

We assign minimal computational resources (1 inference step, Euler solver, ODE integration) to Initial and End states, as these phases require basic positioning in unobstructed space. The Near category receives 5 inference steps with Euler solver and ODE integration, sufficient for approaching objects while avoiding collisions. For Grabbing interactions, we allocate 10 inference steps with Euler and ODE, as these do not require maximal computational resources. Stochastic attempts benefit from controlled variability, so we assign 50 inference steps with SDE integration, which produced optimal performance in the Tool Hang task. Finally, Continuous pushing, requiring the highest precision, receives 100 inference steps with Heun solver and SDE integration to achieve millimeter-precise control.

Category	Characteristics	Inference Steps	Solver	Integration
Initial state (I)	Robot positioned away from targets	1	Euler	ODE
Near (N)	Approaching within 30cm of targets	5	Euler	ODE
Grabbing (G)	Grasping and placing objects	10	Euler	ODE
Stochastic attempts (S)	Precise alignment requiring variability	50	Euler	SDE
Continuous pushing (C)	Sustained precise manipulation	100	Heun	SDE
End state (E)	Objectives achieved	1	Euler	ODE

Table 3: State difficulty categories and their computational requirements

4.6 Adaptive Computation Efficiency

Based on our empirical results across task categories, we mapped state difficulty to optimal computational configurations for each task phase.

Overall, our DA-SIP achieved substantial reductions in task completion time compared to maximum computation baselines: an average 3.3-fold reduction with adaptive CNN, 2.7-fold with few-shot VLM, and 2.3-fold with fine-tuned VLM. Performance remained robust across most methods, with average performance differences of only 1.3%, 4.7%, and 1.8% from maximum computation, respectively. Notably, the fine-tuned VLM achieved an excellent balance between the computational efficiency of CNN-based classification and the deployment flexibility of few-shot VLM approaches. With minimal training data, it achieved consistent performance across environments, even demonstrating significant performance improvements (up to 8% in Tool Hang) while maintaining the adaptability benefits of vision-language models. These results confirm that dynamically allocating computational resources based on state difficulty substantially improves efficiency while preserving task performance, with fine-tuned VLMs offering a particularly appealing balance between reliability and adaptability.

Simulation	SIP		DA-SIP		
	Min Compute	Max Compute	Lightweight CNN	Few-shot VLM	Fine-tuned VLM
Tool Hang	91.02	342.13	106.37 (-3.22x)	150.32 (-2.28x)	139.53 (-2.45x)
Square	25.86	146.68	56.20 (-2.61x)	89.04 (-1.65x)	108.76 (-1.35x)
Transport	73.04	342.54	77.36 (-4.43x)	178.29 (-1.92x)	163.38 (-2.10x)
Push T	1.44	121.89	45.35 (-2.69x)	21.96 (-5.55x)	45.34 (-2.69x)
Lift	57.04	263.28	64.31 (-4.09x)	101.00 (-2.61x)	89.50 (-2.94x)
Can	63.70	214.81	74.32 (-2.89x)	94.94 (-2.26x)	86.44 (-2.49x)

Table 4: Time comparison across different simulations showing computational efficiency gains. Values indicate computation time (seconds), with fold reduction relative to maximum compute shown in parentheses as negative multiples (e.g., -3.2x indicates 3.2x faster than maximum compute). The adaptive configurations achieve notable efficiency, with minimum compute delivering up to **84.6x** reduction in the Push T environment, and Few-shot VLM offering up to **5.6x** speedup. A detailed timing breakdown is provided in Appendix E.2.

Simulation	SIP		DA-SIP		
	Min Compute	Max Compute	Lightweight CNN	Few-shot VLM	Fine-tuned VLM
Tool Hang	25%	25%	27% (+2%)	33% (+8%)	33% (+8%)
Square	88%	90%	92% (+2%)	88% (-2%)	89% (-1%)
Transport	62%	80%	77% (-3%)	62% (-18%)	79% (-1%)
Push T	81%	86%	87% (+1%)	86% (0%)	87% (+1%)
Lift	100%	100%	100% (0%)	100% (0%)	100% (0%)
Can	98%	99%	99% (0%)	99% (0%)	99% (0%)

Table 5: Performance comparison showing generally minimal success rate degradation despite computational savings. Values indicate success rate, with percentage difference relative to maximum compute shown in parentheses. Most configurations maintain performance close to maximum compute, with three environments (Push T, Lift, Can) showing no performance loss with the few-shot VLM approach. The CNN classifier maintains strong performance in Transport (-3% from maximum), while few-shot VLM shows a more substantial performance trade-off (-18%) in this environment.

5 Conclusion

We introduced **DA-SIP**, a *Difficulty-Aware Stochastic Interpolant Policy* that brings adaptive test-time computation to generative robot control. By casting diffusion and flow policies in the stochastic interpolant framework and attaching a difficulty classifier, DA-SIP selects the solver depth, interpolant, and ODE/SDE mode on the fly. Across our simulated manipulation suite, this approach cuts total computation by **2.6–4.4**× while matching the task success rates of fixed, uniform-budget baselines.

This work contributes (i) a unified SI formulation that exposes a rich design space for generative policies, (ii) an adaptive inference system that dynamically selects computational parameters without modifying the underlying policy, and (iii) empirical evidence demonstrating significant computational savings without performance degradation. While our primary evaluation focuses on simulation environments, preliminary experiments with real robot data show that SIP achieves lower mean squared error than diffusion policy on action prediction (Appendix E.5), suggesting promise for physical robot deployment. Future directions include applying this adaptive inference framework to larger robotics foundation models and coupling it with safety monitors for contact-rich tasks. Together, these advances move generative controllers toward efficient, deployable autonomy in resource-constrained physical environments.

Acknowledgments

We thank the authors of Stochastic Interpolant and the SiT for their paper and codebase, which served as the foundation of our research [9, 11]. We are also grateful for the authors of the Diffusion Policy codebase [16], which was instrumental for our implementation.

We thank Sanghyun Woo for valuable early discussions on research methodology and comparative analysis, and Nur Muhammad Mahi Shafiullah for insightful discussions on robotics experiment design and ensuring fair comparisons with baseline methods. We thank Lerrel Pinto and Mark Goldstein for helpful feedback on the draft and experiments. We are grateful to the annotators, including authors, Manish Chowdhury, Elvis Fiador, Jiwon Hwang, Yeonwoo Kim, Bruna Sampaio, and Aditya Singh for their assistance with data annotation. We thank Nanye Ma for helpful discussions about the SiT concepts and codebase, and for valuable feedback on our research approach.

This work was supported by compute resources provided by NYU IT High Performance Computing resources and services.

We also thank the anonymous reviewers for their constructive feedback that helped improve this paper.

References

[1] J. Ho, A. Jain, and P. Abbeel. Denoising diffusion probabilistic models. In *Advances in Neural Information Processing Systems (NeurIPS)*, pages 6840–6851, 2020.

[2] Y. Song, C. Meng, and S. Ermon. Score-based generative modeling through stochastic differential equations. In *International Conference on Learning Representations (ICLR)*, 2021.

[3] Y. Lipman, R. T. Q. Chen, H. Ben-Hamu, M. Nickel, and M. Le. Flow matching for generative modeling. *arXiv preprint arXiv:2210.02747*, 2022.

[4] Michael S. Albergo and Eric Vanden-Eijnden. Building normalizing flows with stochastic interpolants. In *International Conference on Learning Representations (ICLR)*, 2023.

[5] Xingchao Liu, Chengyue Gong, and Qiang Liu. Flow straight and fast: Learning to generate and transfer data with rectified flow. *arXiv:2209.03003*, 2022.

[6] Johan Bjorck, Fernando Casta neda, Nikita Cherniadev, Xingye Da, Runyu Ding, Linxi Fan, Yu Fang, Dieter Fox, Fengyuan Hu, Spencer Huang, et al. Gr00t n1: An open foundation model for generalist humanoid robots. *arXiv preprint arXiv:2503.14734*, 2025.

[7] K. Black, N. Brown, D. Driess, A. Esmail, M. Equi, C. Finn, et al. π_0 : A vision–language–action flow model for general robot control. *arXiv:2410.24164*, 2024. Conference on Robot Learning 2024.

[8] Jason Wei, Xuezhi Wang, Dale Schuurmans, Maarten Bosma, Fei Xia, Ed Chi, Quoc V. Le, Denny Zhou, et al. Chain-of-thought prompting elicits reasoning in large language models. In *Advances in Neural Information Processing Systems (NeurIPS)*, volume 35, pages 24824–24837, 2022.

[9] M. S. Albergo, N. M. Boffi, and E. Vanden-Eijnden. Stochastic interpolants: A unifying framework for flows and diffusions. *arXiv:2303.08797*, 2023.

[10] Tero Karras, Miika Aittala, Timo Aila, et al. Elucidating the design space of diffusion-based generative models. In *Advances in Neural Information Processing Systems (NeurIPS)*, 2022.

[11] Nanye Ma, Mark Goldstein, Michael S. Albergo, Nicholas M. Boffi, Eric Vanden-Eijnden, and Saining Xie. SiT: Exploring flow and diffusion-based generative models with scalable interpolant transformers. In *European Conference on Computer Vision (ECCV)*, pages 23–40. Springer, 2024.

[12] Yang Song, Prafulla Dhariwal, Mark Chen, and Ilya Sutskever. Consistency models. *arXiv:2303.01469*, 2023.

[13] Kevin Frans, Danijar Hafner, Sergey Levine, and Pieter Abbeel. One step diffusion via shortcut models. *arXiv:2410.12557*, 2024.

[14] Nicholas M. Boffi, Michael S. Albergo, and Eric Vanden-Eijnden. Flow map matching. *arXiv:2406.07507*, 2024.

[15] Nicholas M. Boffi, Michael S. Albergo, and Eric Vanden-Eijnden. How to build a consistency model: Learning flow maps via self-distillation, 2025. URL <https://arxiv.org/abs/2505.18825>.

[16] C. Chi, Z. Xu, S. Feng, E. Cousineau, Y. Du, B. Burchfiel, R. Tedrake, and S. Song. Diffusion policy: Visuomotor policy learning via action diffusion. *International Journal of Robotics Research*, 2023. Originally presented at ICLR 2023.

[17] Tony Zhao, Vikash Kumar, Sergey Levine, and Chelsea Finn. Learning fine-grained bimanual manipulation with low-cost hardware. *arXiv:2304.13705*, 2023.

[18] M. Braun, N. Jaquier, L. Rozo, and T. Asfour. Riemannian flow matching policy for robot motion learning. In *IEEE/RSJ International Conference on Intelligent Robots and Systems (IROS)*, pages 5144–5151, 2024.

[19] Aaditya Prasad, Kevin Lin, Jimmy Wu, et al. Consistency policy: Accelerated visuomotor policies via consistency distillation. *arXiv:2405.07503*, 2024.

[20] X. Hu, B. Liu, X. Liu, et al. RF-POLICY: Rectified flows are computation-adaptive decision makers. In *International Conference on Learning Representations (ICLR)*, 2024. Earlier version: NeurIPS 2023 Workshop “Foundation Models for Decision Making”.

[21] X. Hu, Q. Liu, X. Liu, and B. Liu. AdaFlow: Imitation learning with variance-adaptive flow-based policies. In *Advances in Neural Information Processing Systems (NeurIPS)*, 2024.

[22] Anthony Brohan, Noah Brown, Justice Carbajal, Yevgen Chebotar, Xi Chen, Krzysztof Chormanski, Tianli Ding, Danny Driess, Avinava Dubey, Chelsea Finn, et al. Rt-2: Vision-language-action models transfer web knowledge to robotic control. *arXiv preprint arXiv:2307.15818*, 2023.

[23] M. J. Kim, K. Pertsch, S. Karamcheti, T. Xiao, A. Balakrishna, S. Nair, et al. OpenVLA: An open-source vision–language–action model. *arXiv:2406.09246*, 2024. Accepted at NeurIPS 2024.

[24] Michael Ahn, Anthony Brohan, Noah Brown, Yevgen Chebotar, Omar Cortes, Byron David, Chelsea Finn, Chuyuan Fu, Keerthana Gopalakrishnan, Karol Hausman, et al. Do as i can, not as i say: Grounding language in robotic affordances. *arXiv preprint arXiv:2204.01691*, 2022.

[25] Wenlong Huang, Fei Xia, Ted Xiao, Harris Chan, Jacky Liang, Pete Florence, Andy Zeng, Jonathan Tompson, Igor Mordatch, Yevgen Chebotar, et al. Inner monologue: Embodied reasoning through planning with language models. *arXiv preprint arXiv:2207.05608*, 2022.

[26] A. Mandlekar, D. Xu, J. Wong, S. Nasiriany, C. Wang, et al. What matters in learning from offline human demonstrations for robot manipulation. In *Robotics: Science and Systems (RSS)*, 2021.

[27] Nur Muhammad Shafiullah, Zichen Cui, Ariuntuya Arty Altanzaya, and Lerrel Pinto. Behavior transformers: Cloning k modes with one stone. In *Advances in Neural Information Processing Systems (NeurIPS)*, volume 35, pages 22955–22968, 2022.

[28] Pete Florence, Corey Lynch, Andy Zeng, Oscar A. Ramirez, Ayzaan Wahid, Laura Downs, Adrian Wong, Johnny Lee, Igor Mordatch, and Jonathan Tompson. Implicit behavioral cloning. In *Conference on Robot Learning*, pages 158–168, 2022.

[29] Abhishek Gupta, Vikash Kumar, Corey Lynch, Sergey Levine, and Karol Hausman. Relay policy learning: Solving long-horizon tasks via imitation and reinforcement learning. *arXiv preprint arXiv:1910.11956*, 2019.

[30] Greg Brockman, Vicki Cheung, Ludwig Pettersson, Jonas Schneider, John Schulman, Jie Tang, and Wojciech Zaremba. OpenAI Gym. *arXiv preprint arXiv:1606.01540*, 2016.

[31] N. Funk, J. Urain, J. Carvalho, V. Prasad, G. Chalvatzaki, and J. Peters. ACTIONFLOW: Efficient, accurate, and fast policies with spatially symmetric flow matching. In *RSS Workshop “Structural Priors for Learning Robot Dynamics”*, 2024.

[32] Q. Zhang, Z. Liu, H. Fan, G. Liu, B. Zeng, and S. Liu. FlowPolicy: Enabling fast and robust 3d flow-based policy via consistency flow matching for robot manipulation. In *Proceedings of the AAAI Conference on Artificial Intelligence*, volume 39, pages 14754–14762, 2025.

[33] F. Zhang and M. Gienger. Affordance-based robot manipulation with flow matching. *arXiv:2409.01083*, 2024.

[34] H. Liu, C. Li, Q. Wu, and Y. J. Lee. Visual instruction tuning. In *Advances in Neural Information Processing Systems (NeurIPS)*, volume 36, pages 34892–34916, 2023.

[35] S. Bai, K. Chen, X. Liu, J. Wang, et al. Qwen 2.5-vl technical report. *arXiv:2502.13923*, 2025.

[36] A. Kamath, J. Ferret, S. Pathak, N. Vieillard, and Gemma Team. Gemma 3 technical report. *arXiv:2503.19786*, 2025.

Appendix A Implementation Details

This appendix provides key implementation details of our DA-SIP framework.

A.1 Stochastic Interpolant Policy Implementation

Table 6: Stochastic interpolant policy hyperparameters

Parameter	Value	Parameter	Value
Optimizer	AdamW	Weight decay	1e-6
Learning rate	1e-4	Schedule	Cosine decay
Batch size	256	Gradient clipping	1.0
Training epochs	5,000	Checkpointing	Every 50 epochs
Loss function	MSE	EMA rate	0.9999
Prediction targets	Velocity/Score/Noise	LR Scheduler	Cosine decay
Interpolants	Linear/VP/GVP	warmup steps	500

A.2 Lightweight CNN Classifier

Our CNN classifier uses three convolutional blocks followed by fully connected layers:

Table 7: Lightweight CNN architecture and training parameters

Architecture		Training Parameters	
Input	RGB image $32 \times 32 \times 3$	Optimizer	Adam
Conv1	32 filters, 3×3 , BatchNorm, ReLU	Learning rate	1e-3
MaxPool1	2×2 stride 2	Batch size	64
Conv2	64 filters, 3×3 , BatchNorm, ReLU	Epochs	100
MaxPool2	2×2 stride 2	Early stopping	patience=15
Conv3	128 filters, 3×3 , BatchNorm, ReLU	Loss function	Categorical cross-entropy
MaxPool3	2×2 stride 2	Class weighting	Inverse frequency
Flatten	2048 units	Validation split	20%
FC1	256 units, ReLU, Dropout(0.5)	Augmentation	Flip, rotation, color jitter
FC2	6 units, Softmax		

We apply histogram equalization per color channel and use weighted random sampling to handle class imbalance with:

$$\text{weights} = \frac{n_{\text{samples}}}{n_{\text{classes}} \times \text{class_counts}} \quad (8)$$

A.3 Few-shot VLM Classification

We use few-shot in-context learning with the following configuration:

- **Models evaluated:** Qwen-VL 2.5, LLAVA-Next, Gemma 3
- **Method:** Present reference images with labels alongside target image
- **Prompt:** "simply pick the label from the sample images you see in prompt and tell me which one is closest to what you see"
- **Category mapping:**

i	initialize	s	stochastic exploration
n	near	e	end state
g	grab	c	continuous pushing

A.4 Fine-tuned VLM Implementation

Table 8: VLM fine-tuning configuration

Model Configuration	Value	Training Parameters	Value
Base model	Qwen2.5-VL-7B-Instruct	Learning rate	2e-5
Quantization	8-bit, NF4 type	Batch size	32
Language LoRA rank	16	Epochs	12
Vision LoRA rank	8	Optimizer	AdamW
LoRA alpha	32	Weight decay	0.01
Vision LoRA alpha	16	Warmup ratio	3%
LoRA dropout	0.05	Precision	FP16
Target modules	q/k/v/o/gate/up/down proj	Gradient checkpointing	Enabled
Image resolution	224x224	Max sequence length	200 tokens

Appendix B Performance comparison

Table 9: Performance on the “Lift” task comparing DDPM, DDIM, and Linear (SI Policy with linear interpolation) under varying inference steps. We used Euler ODE approximator for trained models for SIP. **Note that this is without distillation for SIP**

Inference Steps	Diffusion Policy (DDPM)	Diffusion Policy (DDIM)	SI Policy (ours)
100	1.00	1.00	1.00
50	1.00	0.99	1.00
10	0.04	0.03	1.00
5	0.03	0.02	1.00
1	0.00	0.03	1.00

Table 10: Success rates on the “Can” manipulation task: Comparing conventional diffusion methods (DDPM, DDIM) with our SI Policy using linear interpolation across different inference step counts. All models employ Euler ODE approximation without distillation.

Inference Steps	Diffusion Policy (DDPM)	Diffusion Policy (DDIM)	SI Policy (ours)
100	1.00	1.00	1.00
50	0.97	0.98	1.00
10	0.00	0.00	1.00
1	0.00	0.00	1.00

Table 11: Representative **PushT** results with **VP** interpolation, using either **Euler** or **Heun**, in **ODE** or **SDE** mode, and varying numbers of steps. Performance (success rate) improves with more sophisticated solvers, showing that each configuration must be carefully tuned for optimal results.

Interpolation	# Steps	ODE / SDE	Approximator	Final Step	Success Rate
VP	10	ODE	Euler	Euler	0.786
VP	25	ODE	Euler	Euler	0.897
VP	50	ODE	Euler	Euler	0.912
VP	100	ODE	Euler	Euler	0.918
VP	100	SDE	Euler	Linear	0.918
VP	10	ODE	Heun	Tweedie	0.881
VP	25	ODE	Heun	Tweedie	0.916
VP	50	ODE	Heun	Tweedie	0.920
VP	100	ODE	Heun	Tweedie	0.922
VP	100	SDE	Heun	Tweedie	0.926

Comparison of Diffusion Policy			
Inference Steps	DP (DDPM)	DP (DDIM)	SI Policy (ours)
10	0.125	0.810	0.881
25	0.214	0.813	0.916
50	0.801	0.812	0.920
100	0.807	0.810	0.926

Table 12: **BlockPush** task success rate with GVP interpolation, comparing different approximators (Euler vs. Heun), ODE vs. SDE approaches, and final step methods. Results show that Heun with Tweedie correction achieves the highest success rates, while ODE performance scales with step count. The bottom section provides a direct comparison with standard Diffusion Policy.

Interpolation	# Steps	ODE / SDE	Approximator	Final Step	Success Rate
GVP	1	ODE	Euler	-	0.026
GVP	10	ODE	Euler	-	0.155
GVP	25	ODE	Euler	-	0.199
GVP	50	ODE	Euler	-	0.195
GVP	100	ODE	Euler	-	0.200
GVP	100	SDE	Euler	Euler	0.204
GVP	100	SDE	Euler	Tweedie	0.205
GVP	100	SDE	Heun	Euler	0.215
GVP	100	SDE	Heun	Tweedie	0.227
Comparison with Diffusion Policy					
Method	Configuration			Success Rate	
Diffusion Policy (DDPM)	100 steps			0.210	
SI Policy (ours)	GVP, Heun, Tweedie, 100 steps			0.227	

Table 13: Performance on the **Transport** task with VP interpolation, comparing different numbers of steps, ODE vs. SDE approaches, and approximators. Results show that performance is highly dependent on sufficient step count, with SDE approaches achieving slightly better performance.

Interpolation	# Steps	ODE / SDE	Approximator	Final Step	Success Rate
VP	10	ODE	Euler	-	0.006
VP	25	ODE	Euler	-	0.758
VP	50	ODE	Euler	-	0.796
VP	100	ODE	Euler	-	0.784
VP	100	SDE	Euler	Euler	0.850
VP	100	SDE	Heun	Tweedie	0.850
Comparison with Diffusion Policy					
Diffusion Policy (DDPM)			SI Policy (ours)		
0.852			0.850		

Table 14: Performance on the **Square** task with VP interpolation, comparing different numbers of steps, ODE vs. SDE approaches, and approximators.

Interpolation	# Steps	ODE / SDE	Approximator	Final Step	Success Rate
VP	10	ODE	Euler	-	0.892
VP	25	ODE	Euler	-	0.950
VP	50	ODE	Euler	-	0.942
VP	100	ODE	Euler	-	0.926
VP	100	SDE	Euler	Euler	0.952
Comparison with Diffusion Policy					
Inference Steps	DP (DDPM)		DP (DDIM)	SI Policy (ours)	
10	0.000		0.928	0.892	
50	0.916		0.943	0.942	
100	0.944		0.962	0.952	

Table 15: Tool Hang performance with VP interpolation across different configurations (averaged across 3 seeds)

Interpolation	# Steps	ODE/SDE	Solver	Success Rate
VP	1	ODE	Euler	0.000
VP	10	ODE	Euler	0.115
VP	25	ODE	Euler	0.345
VP	50	ODE	Euler	0.381
VP	100	ODE	Euler	0.351
VP	10	ODE	Heun	0.342
VP	25	ODE	Heun	0.330
VP	50	ODE	Heun	0.371
VP	100	ODE	Heun	0.364
VP	100	SDE	Euler	0.357
VP	100	SDE	Heun	0.368
Comparison with Diffusion Policy				
Step Count		DP (DDPM)	DP (DDIM)	SI Policy (ours)
1		0.000	0.482	0.000
10		0.000	0.484	0.342
25		0.000	0.486	0.371
50		0.534	0.490	0.381
100		0.484	0.480	0.368

Note: Surprisingly, Diffusion Policy methods perform much better on Tool Hang than SI Policy consistently. DDPM achieves the highest overall success rate (0.534) at 50 steps, while DDIM shows remarkable consistency across all step counts, maintaining 0.48 success even at very low step counts.

Appendix C Data Collection and Annotation

This appendix details our methodology for collecting and annotating the dataset of 20,000 labeled robot states used for training and evaluating our difficulty classification models.

We developed a systematic approach to collect data of robot states across various manipulation tasks. Our data collection protocol was as follows:

C.1 Episode Recording and Frame Extraction

We recorded complete episodes across six simulation environments (Can, Lift, Push T, Square, Tool Hang, and Transport). We extracted frames at regular intervals (every 5th frame) with additional adaptive sampling to ensure representation of critical states (e.g., precise grasping moments). This approach yielded approximately 20,000 frames for annotation.

C.2 Annotation Process

Eight volunteers participated in the annotation process. Each annotator received tutorial videos for how to annotate each image for each task. A custom web-based annotation platform was used to help them annotate and each volunteer is given a distinct username.

C.3 Difficulty Categories

The following categories were used to classify robot states based on computational requirements:

1. **Initial (I):** The robot is positioned away from targets and objects, performing gross positioning movements in free space. No precise control is needed.
2. **Near (N):** The robot is approaching within approximately 10cm of a target object but has not yet initiated contact or grasping. Some care in motion planning is required.
3. **Grabbing (G):** The robot is in the process of grasping an object, or has grasped an object and is moving it to a new location. Moderate precision is required.
4. **Stochastic (S):** The robot is attempting a precise placement or alignment task that requires controlled variability (e.g., inserting a tool, threading a needle). High precision with some exploration is needed.
5. **Continuous (C):** The robot is pushing or manipulating an object without grasping, requiring continuous fine control with millimeter precision (e.g., pushing a block along a specific path).
6. **End (E):** Task objectives have been achieved, and the robot is in a terminal state or moving away from completed objectives.

C.4 Dataset Finalization

To ensure reliability, each state was labeled by multiple annotators. For the final dataset, we assigned category labels using majority voting.

The most common boundary cases occurred between Near (N) and Grabbing (G) categories

These patterns reflect the continuous nature of difficulty transitions during task execution, with some states occupying boundary regions between categories.

The final dataset contains approximately 20,000 labeled states spanning all six difficulty categories across the different simulation environments, providing a comprehensive foundation for training our difficulty classifiers.

Appendix D Robustness/Efficiency Analysis

D.1 Data Efficiency

To address the scalability concern of training the difficulty classifier, especially with the CNN approach, we conducted ablation studies to determine the minimum training data required to achieve comparable performance to our full dataset. We measured the accuracy of models trained on varying numbers of images, evaluating their predictions against majority-vote labels from human annotators.

Table 16: CNN classifier accuracy with varying training data sizes. Test set sizes shown in parentheses.

Environment	Training Images					Test Set Size
	100	200	300	500	2000	
Square	8%	48%	84%	85%	84%	910
Tool Hang	2%	23%	19%	29%	39%	1584
Lift	87%	89%	90%	92%	92%	900
Can	2%	2%	85%	83%	88%	520
Transport	1%	1%	36%	36%	37%	1584
Average	20.0%	32.6%	62.8%	65.0%	68.0%	–

The results show that 300 training images achieve near-plateau performance for Square, Can, and Lift, while Tool Hang peaks at around 200 images and Transport at 300 images. Therefore, approximately 300 images per task can be used as a reasonable baseline amount of training data needed to train an accurate classifier model, especially when training from scratch with architectures such as CNNs.

D.2 Computational Overhead Analysis

We re-rolled out the policy for Tool Hang (88 iterations, per-iteration average):

Table 17: Per-cycle computational breakdown for different difficulty classifiers (in seconds)

Component	CNN	Fine-tuned VLM
Classifier inference	0.023	0.362
SIP policy inference	0.301	0.127
Simulation execution	0.977	0.991
Data processing	0.057	0.055
Total per cycle	1.357	1.535

D.3 Few-shot VLM Learning

To investigate the impact of the number of exemplar images on VLM classification performance, we tested few-shot learning with varying numbers of images per category. The following results demonstrate the trade-off between classification accuracy and inference time.

Table 18: Few-shot VLM performance and inference time with varying exemplar images

Environment	1 img/cat	2 img/cat	3 img/cat
Square	20% (0.55s)	20% (0.89s)	24% (1.26s)
Tool Hang	16% (0.56s)	32% (0.91s)	52% (1.26s)
Lift	57% (0.48s)	83% (0.64s)	83% (0.82s)
Can	25% (0.52s)	43% (0.75s)	38% (1.05s)
Transport	25% (0.50s)	25% (0.72s)	33% (1.05s)
Average	28.6% (0.52s)	40.6% (0.78s)	46.0% (1.09s)

D.4 CNN Robustness to Noise

We also conducted additional experiments evaluating the robustness of our CNN difficulty classifier under noisy sensor conditions. We added varying levels of gaussian noise to test images before classifying. This addresses the concerns about real-world deployment where sensor noise is unavoidable.

Experimental setup:

- Training samples per environment: 300
- Test set: 20% of data (stratified split)
- Random seed: 42 (ensures reproducible noise across runs)
- Noise levels: $\sigma \in \{0.0, 0.05, 0.15, 0.30, 2.0\}$

Table 19: CNN classifier accuracy (%) under different noise levels

Environment	Clean ($\sigma=0.0$)	Low Noise ($\sigma=0.05$)	Medium Noise ($\sigma=0.15$)	High Noise ($\sigma=0.30$)	Extreme Noise ($\sigma=2.0$)
Square	84.51	85.60 (+1.10)	83.08 (-1.43)	78.68 (-5.82)	12.86 (-71.65)
Tool Hang	20.52	20.27 (-0.25)	19.95 (-0.57)	19.63 (-0.88)	1.83 (-18.69)
Lift	91.67	90.67 (-1.00)	89.00 (-2.67)	81.89 (-9.78)	75.11 (-16.56)
Can	81.92	82.50 (+0.58)	82.12 (+0.19)	82.69 (+0.77)	77.69 (-4.23)
Transport	34.66	34.34 (-0.32)	34.60 (-0.06)	35.10 (+0.44)	22.85 (-11.81)
Average	62.66	62.68 (+0.02)	61.75 (-0.91)	59.60 (-3.06)	38.07 (-24.59)

This experiment demonstrates that our CNN models still maintain reasonable performance under high noise conditions ($\sigma=0.30$) with only 3.06% average accuracy drop. $\sigma=2.0$ represents extreme noise conditions beyond typical real-world scenarios.

D.5 Real Robot Training Validation

To address concerns about sim-to-real transfer, we conducted an experiment with the 'real robot pushT' that has publicly available training data. We were able to train a diffusion policy and SIP with linear interpolation and velocity prediction and found a decreasing pattern of training action MSE, revealing that SIP can mimic the expert human demonstrator, which suggests it will be useful when deployed in the real world. Due to time constraints, we were unable to roll out actual robot trajectories.

Experimental setup:

- Dataset: Real robot PushT human demonstrations
- Policy configuration: SIP with linear interpolation and velocity prediction
- Baseline: Diffusion Policy with identical training setup
- Metrics: Training loss and action MSE over training steps

Table 20: Real robot training results

Training Loss			Action MSE		
Step	Diffusion Policy	SIP	Step	Diffusion Policy	SIP
420	0.0760	0.183	420	0.0250	0.0136
2520	0.0238	0.085	2520	0.00582	0.00472
4614	0.0382	0.131	4614	0.00467	0.00294